

Super-solar Metallicity in the NLS1 Galaxy Markarian 1044

Dale L. Fields¹, Smita Mathur¹, Richard W. Pogge¹, Fabrizio Nicastro², Stefanie Komossa³
& Yair Krongold^{2,4}

fields@astronomy.ohio-state.edu

ABSTRACT

The determination of the bulk metallicity and the abundance mixture of various elements is very difficult in quasars and AGNs because only a few lines are observed and the ionization correction is unknown. Most abundance studies of AGNs assume the N/C ratio scales as metallicity (nitrogen goes as metallicity squared) and so serves as a metallicity indicator. We present an accurate metallicity determination of the narrow-line Seyfert 1 (NLS1) galaxy Markarian 1044, using O VI column density measurements from the *Far Ultraviolet Spectroscopic Explorer* (FUSE) together with C IV, N V, and H I from *Hubble Space Telescope* observations. In this absorption line study we find that the circumnuclear gas in Mrk 1044 has a metallicity of at least five times solar. This is consistent with the expectation that NLS1s have a high metallicity, similar to that found in high-redshift quasars. More surprisingly, we find that the absorbing material requires a near-solar mixture. In other words, the N/C is consistent with the solar ratio, and does not scale with the metallicity. This suggests that the chemical enrichment scenario for this object, and perhaps for AGNs in general, may be different from the traditional model of galactic metal enrichment, at least in the high-metallicity regime.

Subject headings: galaxies:Seyfert — quasars:individual(Mrk 1044) — quasars:absorption lines — quasars:emission lines — galaxies:abundances — ultraviolet:galaxies

¹Department of Astronomy, the Ohio State University, 140 West 18th Avenue, Columbus, OH 43210, USA

²SAO, 60 Garden Street, 02138, Cambridge, MA, USA

³Max-Planck-Institut für extraterrestrische Physik, Giessenbachstrasse 1, D-85748 Garching, Germany

⁴Instituto de Astronomía Universidad Autónoma de México, Apartado Postal 70 - 264, Ciudad Universitaria, México, D.F., CP 04510, México

1. Introduction

The study of metallicity, or more precisely, the study of metallicity indicators in AGNs has a long history (e.g. Bahcall & Kozlovsky 1969). The metallicity of material in an AGN has the potential to tell us about the star formation history without looking at the stars themselves, which is very important in such objects as high-redshift quasars where what appears to be solar or above metallicity is thought to be achieved in what must be less than a Gyr. Metallicity studies have also been conducted of the local AGNs, the less powerful Seyferts. While some may consider the enrichment questions less fundamental in these type of AGNs, there are still curious correlations between the metallicity of gas (host) and the luminosity (AGN) (Shemmer & Netzer 2002). While standard Seyferts may have perfectly reasonable metallicity indicators for their host, there are some local AGNs with what appears to be unusually high metallicities: the Narrow-Line Seyfert 1.

The class of AGNs known as Narrow-Line Seyfert 1s (NLS1) are defined by their relatively narrow permitted lines ($< 2000 \text{ km s}^{-1}$) and a weak [O III]/H β ratio (< 3) (Osterbrock & Pogge 1985). Their spectral properties place them at one end of a distribution of AGN properties known as Eigenvector 1 (Boroson & Green 1992). Later studies of their X-ray properties found that their steep X-ray spectra compared to other Seyfert 1s (Boller, Brandt & Fink 1996; Brandt, Mathur & Elvis 1997) continue to place them at one end of this variation in AGN properties.

While it is not yet resolved, it is generally accepted that the physical driver of Eigenvector 1 is the fractional Eddington accretion rate ($\dot{m} = \dot{M}/\dot{M}_{\text{Edd}}$) as suggested by Pounds, Done & Osborne (1995) and Boroson (2002). This would set NLS1s as a class of AGNs that are undergoing heavy relative accretion, in some ways similar to high redshift quasars. Because NLS1s have a similar luminosity distribution as normal Seyfert 1s, this places the central black hole mass of NLS1s as smaller (10^6 - 10^7) than those of standard Seyfert 1s ($(10^8$ - $10^9)$) (Grupe et al. 2004, and references therein). Because there are relationships between the mass/velocity dispersion of a spheroid and the mass of the black hole it is host to (Gebhardt et al. 2000; Ferrarese & Merritt 2000; Merritt & Ferrarese 2001), this indicates that NLS1s lie in galaxies with weak bulges. This may not be completely true as there is some evidence that NLS1s do not tend to lie on the standard $M_{BH} - \sigma$ relation (Mathur et al. 2001; Grupe & Mathur 2004; Mathur & Grupe 2005). NLS1s and high-redshift quasars share steep X-ray slopes as compared to other AGNs (Grupe et al. 2005). Another difference between narrow-line and standard (broad-line) Seyferts is that the emission line metallicity indicator N V/C IV is much stronger in NLS1s (Shemmer & Netzer 2002). If the N V/C IV is to truly be a metallicity indicator, NLS1s should be placed along with high-luminosity (high-redshift) quasars as the most metal rich of all AGNs. While it is not necessarily expected that NLS1s

and QSOs have similar star formation histories, there is no *a priori* reason why NLS1s and broad-line Seyferts should share one. It has been proposed that NLS1s are an evolutionary phase by Mathur (2000) and if so, studying their metallicity may inform us to the evolutionary properties of their host. Even if this hypothesis is invalid, and NLS1s are simply a distinct class of medium-luminosity AGNs, then studying the metallicity is important to try and distinguish why certain bulges host NLS1s instead of broad-line Seyferts.

A problem lies, however, in whether the metallicity indicators studied in fact return the correct metallicity. Unlike in stars, where the physical conditions, input spectrum and localization of various lines are relatively understood, very little is truly well known about AGNs. The paucity of lines and the fact that many of them may arise from unique regions of the AGN with what can be very different conditions does not assist our situation either. Additionally, historically metallicity studies have primarily used emission lines, for the simple reason that these were all that were available or feasible. And on an order of magnitude basis, a stronger emission line should correspond to more of a particular species. Line ratios should give information about the relative quantities of particular elements. Unfortunately this can be muddied by the shape of the ionizing spectrum or lines coming from physically separate regions (just to name two problems). Absorption line studies, being insensitive to effects such as geometry or density, offer a better measure the quantity of a species. While absorption line studies are not feasible on survey scales, a few detailed analyses of individual systems have the potential to provide a sort of “anchor” to the much more widespread emission line measurements.

In this paper we aim to define the relative (and absolute) abundances for a few common elements in the NLS1 galaxy Mrk 1044. To this end, this nearby AGN ($z = 0.01645$) has been observed with the FUV spectrograph onboard the *Far Ultraviolet Spectroscopic Explorer* (FUSE) satellite. Even with absorption line studies, however, the ionization correction remains a major problem in transforming the observed ionic column densities to a true abundance. This problem is relatively common in any study that only covers a small wavelength region and/or contains information on few species of a particular element. For this reason, we extend the baseline of observed species in Mrk 1044 by adding O VI in the FUV range to measurements made in a STIS study at approximately the same epoch (Fields et al. 2005, henceforth F05). Neither dataset alone could break the inherent degeneracies in making the photoionization correction, but both datasets together select a small region of parameter space from which we can determine the metallicity of this system. In §2 we detail the observations made and the data reduction path followed. In §3 we give the methods with which we analyse the data. We finish in §4 with our conclusions.

2. Observations and Data Reduction

Mrk 1044 was observed by the Far Ultraviolet Instrument onboard the Far Ultraviolet Spectroscopic Explorer on UTC 2004 January 01 and 02. The observation was conducted over one ≈ 7 hour observation from MJD 53005.74609375 to 53006.046875. The data sets are D0410101. The received data was reduced by the standard CalFUSE pipeline. The FUSE IDL tool FUSE_REGISTER was used to cross-correlate, weigh, and coadd the spectra. We use the observations with the 1A detector and the LiF mirror in this analysis.

3. Analysis

The UV spectrum observed by FUSE appears as most AGN spectra do, as can be seen in Figure 1. The continuum is essentially flat, with a slope indistinguishable from zero (expressed as $\alpha = 0.0$ in $f_\nu \propto \nu^{-\alpha}$). The AGN imprints two emission line complexes, the most obvious being the blend of Ly β and O VI $\lambda\lambda 1032, 1038$ observed from 1030 to 1060Å. The other, much weaker, is N III $\lambda\lambda 990, 992$ observed around 1010Å. There are also many absorption lines, most of which are Galactic in origin, but some of which are the result of systems intrinsic to Mrk 1044.

The purpose of this paper lies in the absorption lines intrinsic to Mrk 1044, but this is complicated by the presence of so many Galactic absorption lines. As many absorption lines in an AGN spectrum are the result of outflowing material with high relative velocities, line identification must begin with locating known Galactic lines so as to avoid contamination. The Galactic source causing the most absorbing features is molecular hydrogen (H₂) in the ISM. We use the template used in Romano et al. (2002) to model the H₂ absorption lines. We then use line lists such as those in Sembach (1999) to identify the Galactic metal lines C II $\lambda\lambda 1036, 1037$, O I $\lambda 1039$, Ar I $\lambda 1048$, and Fe II $\lambda\lambda 1055, 1063$. Then, guided by the results of F05, we constructed velocity maps, such as can be seen in Figure 2. We adopt the NASA/IPAC Extragalactic Database (NED) value of the systemic velocity of Mrk 1044 of 4932 km s⁻¹. This figure covers the same ranges as Figure 3 in F05, and shows what are likely the same absorbing systems as in Ly α , N V, and C IV, the strong System 1 at -1158 and the weaker System 2 at -286 km s⁻¹. Figure 2 illustrates the danger of not fully identifying Galactic lines before doing a velocity study. The feature at ≈ -200 appears to be an absorbing system in all but N III $\lambda 990$. However, what appears to be the O VI $\lambda 1032$ line is really Ar I $\lambda 1048$. In addition, the Ly β at the redshift of System 1 is heavily blended with a H₂ line at 1048Å. This figure also shows what is missing: no N III absorption lines are present at the positions of System 1 or 2, and no Ly β is found at System 2. We note that there appears to be an absorption system at $v \approx 0$ km s⁻¹ relative to the systemic velocity

of Mrk1044 in O VI. The Ly β spectrum at that velocity neither supports nor opposes such a determination. However, F05’s Figure 3 clearly shows that neither C IV nor N V have absorption at that velocity, though Ly α is consistent with the presence of an absorber. It is possible that this is a highly ionized system, but because we cannot extract reliable information about it due to its scarcity of absorption lines, we do not consider it further.

Measurements of the properties of these lines proved too difficult to accomplish by modeling the emission and absorption lines along with a H₂ template simultaneously in the STSDAS package SPECFIT (Kriss 1994). This was mostly due to two factors: 1) the unsuitability of gaussians to properly model the emission line profiles, and 2) the inability of the H₂ template to successfully model the Galactic absorption line complex. Five gaussians were found to adequately (but not satisfactorily) fit the blend of Lyman β and O VI. However, the best fit solution was often not physically acceptable, one example of which was the tendency of the two broad O VI lines, when left unconstrained, to centroid themselves asymmetrically (i.e. both “inside” or “outside” the two narrow O VI lines). The H₂ template failed to simultaneously fit both the strong and weak lines.

Because the good measurement of these features with problems (emission lines and H₂) are ancillary to the goal of well measuring the intrinsic absorption systems, we attempt to remove the presence of these problems one at a time. To solve the issue of the emission lines, we fit, by eye, a spline to the emission line structure and normalize the spectrum by dividing by this “pseudo-continuum.” Such a normalized spectrum can be seen in Figure 3. This spectrum is obviously not perfectly fit everywhere (notice the poorly normalized flux near 1059Å), but does well enough around the positions of the absorption lines we are measuring. We then subtract an H₂ template fit. At this point, the lines intrinsic to Mrk 1044 as well as the Galactic metal lines can be fit. Unfortunately, while normalizing the spectrum worked well to solve the problem of the poorly fitting emission lines, the issue of the H₂ fitting was never solved to our complete satisfaction. When the weaker H₂ lines were fit to, the template predicts completely black cores for the strong lines which is not reproduced in the data. Also somewhat related to this is that the model’s strong lines have too weak wings. Increasing the model column density to fit the wings of the data again produces black cores, and fitting to the core of the strong lines “creates” two absorption lines at the wings out of the residuals. The blackness issue may be caused by the data. As Figure 3 shows, all the strong absorption lines (most of them due to H₂) reach a minimum around 0.15, which may indicate a miscalibration in the flux. However, the bottoms of all these lines are already (individually) consistent with zero. Also, resetting the flux lower does nothing to solve the wings issue because all of these lines lack multi-pixel troughs (which fitting to the wings predict). Because of this unresolved problem, we warn against trusting the H₂ subtraction, which will affect the fidelity of any lines molecular hydrogen is blended with such as the

Lyman β line of System 1 as well as Galactic C II and C II* at 1036 and 1037 Å.

We perform two separate analyses on the data. The first is a standard line fitting which gives us the observational parameters (equivalent width, centroid, line width) and terminates in the estimation of the column density via the curve of growth technique described in Spitzer (1978). The second directly integrates over the line structure to give us the column density via the apparent optical depth technique laid out in Savage & Sembach (1991). Comparing the results of these two separate methods will give us additional insight into whether these lines give trustworthy results. We feel confident in the utility of these methods even though studies such as Arav et al. (2005) have found that some absorption features are inhomogeneous systems. System 1 as shown in F05 is well sampled and is very well fit by a gaussian profile across the entire line. The excellence of such a simple model fit implies that we are dealing with a kinematically simple system (a single absorber). Unfortunately, System 2 is weak enough that it has much more noise in its profile, but it is not the focus of this investigation, nor does it figure into our conclusions in §4.

The spectra are normalized in the analysis package LINER (Pogge & Owen 1993). We also use LINER to derive an initial estimate of the properties of the lines. The resultant fits of this program were then used as the inputs for the SPECFIT package. This returns our final values of the equivalent widths, line centroids, and line widths. Equivalent widths were then converted into column densities through the curve of growth method. We calculated the column density for velocity spread parameter b -values of 10, 20, 40, and 80 km s⁻¹, but we report only the value derived from $b = 20$ as that value gives consistent results between the O VI doublet and was also the value used in F05. The line centroiding is limited by localized detector distortions. The galactic absorption lines show the absolute velocities should be shifted positively by about 3-5 km s⁻¹, while the FUSE White Paper on the subject shows that the relative wavelength errors where our lines are located are about 8 km s⁻¹. We use this as our centroiding error.

To determine if the apparent optical depth method is appropriate, we first test whether a line is resolved ($\Delta\lambda_{obs} \geq 2 \Delta\lambda_{lsf}$). We compare FUSE’s instrument profile of ≈ 20 km s⁻¹ with the line widths returned from the SPECFIT package. A stricter test is for the line to be definitely resolved, in other words more than three standard deviations above the nominal resolution limit. If a line passes these tests, we use the normalized residual flux (I_r) that results from the LINER fit and integrate over the line.

We have determined two major sources of uncertainty in our line parameters. The first is the standard photon noise one expects and can be propagated through each stage of the analysis process. The second is that associated with a sub-optimal fit to the pseudo-continuum. We determine this by making not one, but nine by-eye spline fits in LINER

to the emission line complex. These nine fits will result in nine different final values of each line parameter. We take the mean of each set of nine values as the true determination of that parameter. The scatter of the nine values around that mean is then used as the second component in our uncertainty. In all nine cases, the fit to the pseudo-continuum is reasonable, but several were purposefully fit to the outer envelope of the noise. The two components of the uncertainty are then added in quadrature to give the final value of the uncertainty provided in this paper.

3.1. Mrk 1044 Emission Lines

While this paper is focused around the absorption line results, we measure and report the emission line measurements so as to place the level of Mrk 1044’s metallicity in the broader context of most AGN metallicity studies in which it is not feasible to measure the absorption line properties. The parameters for the observed emission lines can be found in Table 1. Given for each line (Lyman β , N III, and O VI) are the equivalent widths, the gaussian FWHM for any components they have, and the velocity offset from systemic. In general, the emission lines are offset by hundreds of km s^{-1} to the blue. There does not appear to be a consistent velocity offset among the emission lines. The N III doublet is weak enough so as to be fit with a single gaussian each, while the O VI doublet requires a narrow and broad component each. The Lyman β line only requires a broad line; a narrow line does not significantly improve the overall fit. In general, gaussians adequately, but not well fit the data. As discussed above in §3, if left completely unconstrained the model of the absorption lines returned very unphysical results with regards to the doublets. To ameliorate this, for each doublet the naturally weaker of the lines is pinned to the stronger. We pin the width and the wavelength, but leave the relative fluxes unpinned because otherwise the model cannot even adequately fit the data. Due to the absence of a narrow component to Lyman β and because it is blended with O VI, one may ask if it is properly identified. Evidence in favor of such an identification is: 1) a four-component fit to the O VI complex (2 narrow, 2 broad) always leaves an excess of blueward flux, 2) a six-component fit (3 per O VI) is not sufficiently superior to a broad Ly β + four-component O VI and 3) the centroid of the component blueward of the O VI is generally consistent with the redshift of the other emission lines (Ly β , O III).

3.2. Mrk 1044 Absorption Line Systems

We report good (3σ) detections of four lines belonging to absorption systems intrinsic to Mrk 1044. We find a velocity for System 1 of -1158 km s^{-1} and a velocity for System 2 of -286 km s^{-1} relative to the systemic velocity of Mrk 1044. These lines are consistent with the systems found in F05, which reported velocities of -1158 and -286 km s^{-1} (a perfect match!). The velocities of each individual line also match well with the mean velocities. In the case of System 2, the weaker of the O VI lines is not detected at $> 3\sigma$. Table 2 gives the measured and calculated parameters for these absorption systems: the observed wavelength, the FWHM, the equivalent widths, the calculated column densities (by both the curve of growth and apparent optical depth methods) and the velocity offset from the systemic. For the lines that are not resolved (System 2's) we give only the column density derived from the curve of growth method. For System 1 we also give the apparent optical depth column density, though it should be noted that only the O VI lines are definitely resolved ($> 3\sigma$ above the $2 \Delta\lambda_{lsf}$ limit which is about 40 km s^{-1}). Additionally, the 3σ upper limits on the undetected N III lines are given.

To determine the column densities with the apparent optical depth method, we first calculate the covering fraction (C_f) of each of these two systems following Hamann et al. (1997). However, there is a problem in that O VI $\lambda 1038$ (I_1 in their formalism) has a lower value of the normalized flux in its trough than O VI $\lambda 1032$ (I_2), on average about 0.10 to 0.15, respectively. This is unphysical, and we attempt to solve this problem by modifying the lines as follows. We note that the errors on points in these two troughs are about 0.05, and we calculate two covering fractions, one where the trough of I_2 is lowered by one sigma, and one where the trough of I_1 is raised by one sigma. This allows seemingly reasonable values of the covering fraction to be found, typically around 0.91 and 0.86 for the two methods. Unfortunately, the covering fractions are often barely too small in the majority of cases where I_2 is lowered. We report the values derived from increasing the trough of I_1 by one sigma as our values of O VI. In the case of O VI $\lambda 1032$ the calculation of the optical depth just fails ($C_f + I_{trough} = 1$). For this line we average over the seven calculable results. While this line has an uncertainty on its column density even greater than its value, it should be noted that it matches the value from the other line well. The covering factor for System 2 is, by the formalism, set to 1 since $I_2 < I_1^2$. While this is also unphysical, such a result is not unexpected due to this system being unresolved, let alone minimally detected. This result merely tells us that we have no information about the covering fraction for this line.

The value of the covering fraction for System 1's O VI is different than that found for C IV and N V. As just given above, we find a value of about 0.86 for O VI, while the derived values for the other lines are approximately 0.72. One solution is that the location

in the broad-line region (BLR) that the O VI emission line flux comes from is sufficiently closer to the central black hole than the location that produces the C IV and N V. The absorbing gas (System 1), being of finite size, will likely completely cover the continuum source, mostly cover the O VI emitting region, and cover to a lesser degree the C IV and N V emitting region. Such a toy model could explain the observed covering fraction for these three species. For this reason we do not consider this discrepancy in covering fraction a problem to be corrected.

There is one major caveat that must be addressed with regards to the measurement of the Ly β line of System 1, namely that this line is heavily blended with a galactic H₂ line. Given the difficulty in subtracting the H₂ (see §3), one can see how difficult getting an accurate value of the H I column density is. The uncertainties in the measurements of its properties are very large compared to the other absorption lines, reflecting this. What isn't reflected in those uncertainties is any systematic effect. Comparing to the Ly α derived values from F05, we find that the Ly β value of H I is much higher, by a factor of 2-4. If this is so, the H₂ at this location is under-subtracted, which matches the effect on the strong H₂ lines. In this case, our Ly β derived value should represent more of an upper limit on the total H I column. Because which H I value we decide to take will affect our metallicity measurements (in magnitude, but not in direction or in general effect) later in §4, we wish to point out that there is no reason to trust the Ly β column above that of the Ly α . As Figure 4 of F05 shows, the Ly α line is symmetric and appears clean of contamination from coincident lines. Its profile does not suggest saturation and the continuum around is well-normalized.

To determine the elemental column densities from the ionic column densities, we must make an ionization correction. To do so, we use the photoionization-equilibrium code Cloudy94¹ (Ferland et al. 1998). This code creates a model of gas in equilibrium with an incident flux. From this, we take the predicted column densities of various species for specific input conditions and compare them with the data. The four inputs to Cloudy we are concerned with are 1) the incident spectral energy distribution (SED), 2) U , the ratio of the number densities of ionizing photons to particle (H) density at the surface of the modeled cloud, 3) the abundance ratios in the gas cloud, and 4) N_H , the column density of hydrogen through the cloud. Throughout our analysis we keep the SED and the assumed metallicity the same and vary U and N_H . For the SED we focus on Cloudy's standard AGN template for much of our analysis, and for abundances we select solar in level and in mixture also for most of our analysis. We then calculate the column densities of various ions at a grid of 0.01 spacing in both $\log U$ from -2 to 0 and $\log N_H$ from 18 to 20 .

¹Cloudy version C94.00, obtained from the Cloudy webpage <http://www.nublado.org/>

We then look for models which predict column densities in agreement with all those measured. In this study we did find the column density of O VI. We are not, however, able to determine the physical parameters of this absorber with just this single species. In addition to this information found by FUSE observations, we bring into this study the column densities of H I, C IV, and N V found by using STIS in F05² The column densities of C IV and N V are 14.47 ± 0.06 (C IV) and 14.46 ± 0.02 (N V). Because Ly α is not a doublet, its covering fraction cannot be truly determined. Since we determine different covering fractions for multiple doublets, we cannot just assign it a covering fraction determined from other lines. Instead, we find the column density of H I for a range of covering fraction from 0.75 to 1.00. The results are shown in Figure 4. In this figure the models which match the observed column densities to within one sigma are shaded for each ion. One can see that there is a small region of parameter space around $\log U = -1.29$, $\log N_H = 18.85$ where all three of the metals agree to within one sigma. There is no location, however, in which the three metal lines and the hydrogen agree.

We also investigate how the choice of incident SED affects our results. We use SEDs of two NLS1s (Ark 564 and NGC 4051) and find qualitatively the same result, though the agreement of the three metal lines takes place at the 3-3.5 σ level. Compared to Figure 4, all metals shift to lower $\log U$ values, the magnitude of which is highest for Oxygen, small for Nitrogen, and smallest for Carbon, about 1.0, 0.5, and 0.3 dex respectively. Additionally, the amount of H I for a particular $\log U$ shifts to lower N_H , between 0.4 and 0.6 dex. We also decrease the amount of flux coming out in the EUV (an unobservable region of the spectrum) to test its effects and find that the magnitude of its changes is small compared to the SED differences between the standard “table agn” and the the two NLS1s. We also test non-solar abundance mixtures by increasing the nitrogen by factors of two and four. We find at the 3 σ level our data is consistent with overabundant Nitrogen at twice the solar mixture, but inconsistent with four-times-solar.

3.3. Galactic Absorption Lines

The interstellar medium imprints absorption lines belonging to molecular hydrogen, C II, O I, Ar I, and Fe II. The measured parameters of these lines are given in Table 3. Given are the ions, their rest and observed wavelengths, the FWHM, equivalent width, column densities via the two methods, and the relative velocity (to zero). We also give the

²The values of the covering fraction in that paper had an error, resulting in low column densities of C IV and N V. The correct mean values as reported in the erratum are also quoted here.

value for the H_2 column density as fit to the weak absorption lines. The two C II lines were blended to some degree with H_2 , C II* especially, and the fit was unstable in SPECFIT. Additionally, the values of the column density between the two carbon lines are inconsistent for all values of b . For that reason, only their observed parameters (EW, FWHM, v_{rel}) are given in the table. We are not able to give column density values for the two Fe II lines as their f -values are not available (curve of growth method) and neither are definitely resolved (apparent optical depth method). In addition, the redward Fe line ($\lambda 1063\text{\AA}$) is blended in its wings with H_2 . This leaves us with only O I and Ar I with possible column density values. The O I line appears to be definitely resolved, so we give its column density via the apparent optical depth method. Unfortunately, this leaves us without multiple lines from a single species, which means we are unable to determine the correct b parameter and thus we cannot find the column density via the curve of growth. Calculating the column density for O I for multiple b values gives a best match to the apparent optical depth column density at b between 20 and 40 km s^{-1} . Unfortunately, O I $\lambda 1032$ as found in F05 has contradictory parameters. As mentioned in that study, O I $\lambda 1032$ is found in the low-resolution G140L spectrum and is possibly a blend. For this reason, there is no b value consistent with the O I from both studies. With this in mind, we simply return column densities for a b value of 20 km s^{-1} and remind the reader about possible accuracy issues. One should also note that the three clean lines (O I, Ar I & Fe II1055) have a velocity consistent with zero, while the three other lines have the most discrepant velocities and are also the lines blended with H_2 .

3.4. Intergalactic Absorption

On account of the findings in F05, we search our data for the presence of intergalactic absorption lines. In that paper three Ly α forest lines were discovered (see their Table 5). Assuming no saturation (still on the linear part of the curve of growth), the expected equivalent width of the strongest Ly β line would be about 40 m \AA . The three sigma detection in this region is around 100 m \AA . Regardless, there are two absorption features that may be the Ly β counterparts of the two stronger of the Ly α absorption systems. The weakest of the three Ly α systems lies coincident with the blend of Galactic H_2 and C II lines and given the problems with deblending described above in §3 along with its just-three-sigma detection in F05, the recovery of it should be unreasonable. The other two Ly α systems should have corresponding absorption in Ly β at 1033.0 and 1035.8 \AA , and we find two systems at 1033.1 and 1035.7 \AA with equivalent widths of 105 and 80 m \AA . By this measure, the weaker line is not definitely detected and the stronger is very close to the nominal three sigma limit. It should be noted that at the location of the stronger line the pseudo-continuum is at an apparent minimum, lying between the O VI emission line and some excess flux that rises towards the

blue for about 5\AA (see Figure 1). The normalization of this region is very uncertain and contributes a 20 m\AA uncertainty to the overall equivalent width error budget. Combined with the photon noise error, this pushes the detection of the stronger of the lines below the three sigma limit. While both of these features are in the correct locations to be the $\text{Ly}\beta$ counterparts to the low-redshift $\text{Ly}\alpha$ forest lines found in F05, the quality of the spectrum at this location is not sufficient to state a definitive confirmation. Were these the $\text{Ly}\beta$ lines, their strengths would be much larger than expected, but still consistent at the two sigma level (indeed consistent with zero at the three sigma level). For this reason we suggest the $\text{Ly}\alpha$ determined values for this system stand as the measurement of these systems.

4. Discussion and Conclusions

As shown in §3.2, there is no one set of input conditions from which Cloudy can create a model that reproduces all of the observed column densities of the associated absorption lines. This indicates that one or more assumptions made in the creation of those models must be incorrect. The fact that there is a model ($\log U = -1.29, \log N_H = 18.85$ with the standard Cloudy AGN SED) which is extremely satisfactory in predicting the column densities of all the metal species, but not that of H I provides one answer. If the bulk metallicity is in fact about 0.7 dex higher (i.e. N_H really 18.15), then all measured lines (assuming $\text{Ly}\alpha$ has $C_f \approx 0.75$) are in excellent ($< 1\sigma$) agreement. The fact that there is one point that all three metal species agree so well at indicates a good probability of having a solar mixture. With a bulk metallicity around five times solar (+0.7 dex) this is inconsistent with the concept of N/O scaling like O/H (Hamann & Ferland 1999, and references therein), at least for this object. If nitrogen did scale with metallicity, then, under this solution, the N V curve in Figure 4 should lie as far above the C IV-O VI agreement point as the H I lies below it, which it clearly does not. The best-fit Nitrogen is at most 0.06 dex above such a point. At most, Nitrogen can be overabundant with respect to the solar mixture at the factor of two level, above which it shares no model in common with both Carbon and Oxygen. Understandably then, this paper gives a much different value of Z than that found in F05 (minimum ≈ 1.5 solar) where it was assumed that $N \propto Z^2$.

The effects on the metallicity by the SED chosen can be large. As mentioned in §3.2, the metal lines shift to lower values of $\log U$ when a NLS1-specific SED is used, the result of which is that the agreement point is around $\log U = -1.7$. The major change, however, is the shift of H I to lower values of $\log N_H$ which does raise the inferred value of the metallicity by another factor of 2-4 (between 10 and 20 times solar) with the SED of NGC 4051 providing the highest metallicity. To confirm these extremely high values of the metallicity we rerun

Cloudy with the metals set to five or ten times the solar value for the standard and NLS1 SEDs respectively. To be fully self-consistent, we also take Helium enrichment into account. For one model of Helium enrichment ($\Delta Y/\Delta Z = 2$) and bulk metallicity around ten times solar, $\log(He/H) \approx -0.52$. Including this effect does not change our inferred metallicities, but it does shift the best-match $\log U$ to slightly higher values. At the increased metallicities, the metal lines are put into agreement with the H I, though this point is also at larger values of $\log U$ (cumulative with He effects). For the standard AGN SED, we find $\log U = -1.20 \pm 0.04$, $\log N_H = 18.13 \pm 0.02$, and $Z = 5_{-1}^{+2}$ solar metallicities. For the Ark 564 SEDs we find $\log U = -1.55 \pm 0.03$, $\log N_H = 17.86 \pm 0.02$, and $Z = 17_{-3}^{+5}$. For the NGC 4051 SED we find $\log U = -1.68 \pm 0.03$, $\log N_H = 17.85 \pm 0.02$, and $Z = 22_{-4}^{+7}$. The χ^2 surface for the standard AGN SED with solar metallicity is shown in Figure 5 and for the standard AGN SED with five times solar metallicity in Figure 6. The lines of constant χ^2 are projected into the $\log U$ - $\log N_H$ plane. The smoothness and parabolic shape of the χ^2 surface indicate that we have well-sampled the parameter space.

For completeness’ sake, we remind the reader that we have used the Ly α -derived value of H I which is much smaller than the Ly β -derived value. Even assuming that the Ly β value is the correct one (which we conclude should not be done), the inferred bulk metallicity is +0.3 dex (twice solar) using the same arguments.

This study also reinforces that one cannot confine oneself to a small section of the electromagnetic spectrum if one wants to accurately model the physical conditions in these absorbing systems. If one created the same models as we did in this study, but only used the F05 data and assumed $N \propto Z^2$, one would conclude $\log U \approx -1.8$, as that is where the N V and H I are equidistant from C IV. While one would infer a metallicity value approximately +0.7 dex, the physical conditions would be very different and the photoionization correction for other species could be quite wrong. It is only because we have FUSE and HST data that we are able to determine the correct physical conditions and thus the abundance level and mixture.

With the results from the absorption lines, we can finally compare this to the values expected of the emission lines and check for agreement. We compare to the line ratios formalism given in Hamann et al. (2002). We note that the solar mixture used in Hamann et al. (2002) is with the earlier, more metal rich values. If the new values for the solar metallicity are to be used, the metallicities referenced here should be considered about -0.11 less as per Baldwin et al. (2003). The emission line ratios in common (using this study’s and F05’s corrected values) are N V/He II, N V/C IV, N V/O VI, and N V/(C IV+O VI). We also have a measurement of N IV], but Hamann et al. (2002) find the metallicities derived from it to be discrepant, as do we. We therefore exclude it from this comparison. Ratios involving

N V do surprisingly well, indicating a metal rich gas of +0.7 to +0.8 on average, very close to our absorption line values using the standard AGN SED. This is curious, however, in that these emission line models assume $N \propto Z^2$ which is very inconsistent with the results of this absorption line study, and yet get the same value of the bulk metallicity. In other words, emission line ratios based off of N V (such as N V/C IV) appear to be good indicators of Z , but perhaps for the wrong reason for this particular system under investigation. Compared to the NLS1 SEDs, however, the emission line ratios fare rather poorly.

The results of this abundance study are somewhat surprising, not because of the super-solar bulk metallicity found (which was already expected), but because of the solar mixture, especially nitrogen relative to carbon and oxygen. Theoretical models and observations around solar metallicity have nitrogen scaling like Z^2 ($[N/O] \propto [O/H]$) because the CNO cycle will preferentially convert oxygen and carbon into ^{14}N , enhancing nitrogen relative to the other metals over long timescales (Hamann & Ferland 1999, and references therein). This theory then goes against our expectations for Mrk 1044. One would assume that a local spiral galaxy such as Mrk 1044 would have had constant star formation over the past age of the universe, and therefore have nitrogen scaling as Z^2 . There exists, then, a contradiction between our data and theory. One way to reconcile this would have some special enrichment process occur in the nucleus of Mrk 1044 which would enhance the metallicity level and mixture to that which we observe. Another is that the existing models are simply not appropriate to this system. The theory which predicts N going like Z^2 results from studies near solar metallicity. It is fair to say that a metallicity of +0.7 to +1.0 (such as in Mrk 1044) is a far extrapolation from the data these trends are based upon. Additionally, we find that metal mixtures such as we find are not unprecedented for high metallicity stars. A recent study of planet-bearing stars (i.e. metal-rich stars) by Ecuivillon et al. (2004) finds that $[N/H]$ scales with $[Fe/H]$ ($[N/H]/[Fe/H]$ slope is consistent with zero at the two sigma level) over the range $-0.4 < [Fe/H] < +0.4$. Said study stops short of the significantly super-solar status of this Seyfert since the set of such stars simply subsides. Thus our result can simply be a continuation of an existing observed trend in enrichment. This, like the $N \propto Z^2$ theory, hinges on an extrapolation, though not nearly as large a one. With the dearth of Galactic studies at extremely high metallicities, Mrk 1044 can provide a calibration point not only for AGN metallicity studies, but also for enrichment theory.

The authors wish to thank Marc Pinsonneault for discussions involving metal enrichment and star formation histories. This research has made use of the NASA/IPAC Extragalactic Database (NED) which is operated by the Jet Propulsion Laboratory, California Institute of Technology, under contract with the National Aeronautics and Space Administration. Primary support for this work was provided by NASA grant NNG04GI04G.

REFERENCES

- Arav, N., Kaastra, J., Kriss, G.A., Korista, K.T., Gabel, J., Proga, D. 2005, ApJ, 620, 655
- Bahcall, J. & Kozlovsky, B.-Z. 1969, ApJ, 155, 1077
- Baldwin, J.A., Hamann, F., Korista, K.T., Ferland, G.J., Dietrich, M., & Warner, C. 2003, ApJ, 583, 649
- Boller, Th., Brandt, N., & Fink, H. 1996, A&A, 305, 53
- Boroson, T. 2002, ApJ, 565, 78
- Boroson, T. & Green, R. 1992, ApJS, 80, 109
- Brandt, N., Mathur, S. & Elvis, M. 1997, MNRAS, 285L, 25
- Ecuivillon, A., Israelian, G., Santos, N.C., Mayor, M., Garcia Lopez, R.C., Randich, S. 2004, A&A, 418, 703
- Ferland, G. J., Korista, K. T., Verner, D. A., Ferguson, J. W., Kingdon, J. B., Verner, E. M. 1998, PASP, 110, 761.
- Fields, D., Mathur, S., Pogge, R.W., Nicastro, F., & Komossa, S. 2005, ApJ, 620, 183
- Ferrarese, L., & Merritt, D. 2000, ApJ, 539, L9
- Gebhardt, K., et al. 2000a, ApJ, 539, L13
- Grupe, D. & Mathur, S. 2004, ApJ, 606L, 41
- Grupe, D., Wills, B.J., Leighly, K.M., & Meusinger, H. 2004 AJ, 127, 156
- Grupe, D., Mathur, S., Wills, B.J., & Osmer, P. 2005 AJ, submitted
- Hamann, F., Barlow, T.A., Junkkarinen, V., Burbidge, E.M. 1997, ApJ, 478, 80
- Hamann, F. & Ferland, G. 1991, ARA&A, 37, 487
- Hamann, F., Korista, K.T., Ferland, G.J., Warner, C., & Baldwin, J. 2002, ApJ, 564, 592
- Kriss, G.A. 1994 in Astronomical Data Analysis Software & Systems III, A.S.P. Conf. Series, Vol. 61, ed. D. R. Crabtree, R. J. Hanisch, & J. Barnes (Astronomical Society of the Pacific: San Francisco), p. 437.
- Mathur, S. 2000, MNRAS, 314, L17

- Mathur, S., Matt, G., Green, P.J., Elvis, M., Singh, K.P. 2001, *ApJ*, 551L, 13
- Mathur, S. & Grupe, D. 2005, *A&A*, in press
- Merritt, D., & Ferrarese, L. 2001, *ApJ*, 547, 140
- Osterbrock, D.E. & Pogge, R.W. 1985, *ApJ*, 297, 166
- Pogge, R.W., & Owen, J.M. 1993, *LINER; An Interactive Spectral Line Analysis Program*, OSU Internal Report 93-01
- Pounds, K., Done, C., & Osborne, J. 1995, *MNRAS*, 277, L5
- Romano, P., Mathur, S., Pogge, R.W., Peterson, B.M. & Kuraszkiwicz, J. 2002, *ApJ*, 578, 64
- Romano, P., Mathur, S., Turner, T.J., Kraemer, S.B., Crenshaw, D.M., Peterson, B.M., Pogge, R.W., Brandt, W.N., George, I.M., Horne, K., Kriss, G.A., Netzer, H., Shemmer, O., Wamsteker, W. 2004, *ApJ*, 602 635
- Savage, B.D. & Sembach, K.R. 1991, *ApJ*, 379, 245
- Sembach, K. 1999 in *Stromlo Workshop on High-Velocity Clouds*, A.S.P. Conf. Series, Vol. 166, eds. B.K. Gibson & M.E. Putman p. 243
- Shemmer, O. & Netzer, H. 2002, *ApJ*, 567, L22
- Spitzer, L. 1978, *Physical Processes in the Interstellar Medium* (New York: Wiley-Interscience), 46

Table 1. Emission Line Properties of Mrk 1044

Ion	λ_{Rest} [Å]	Equivalent Width [Å]	FWHM [km s ⁻¹]	Velocity [km s ⁻¹]
N III	990	0.68 ± 0.15	341 ± 54	-190 ± 8
N III	992	0.55 ± 0.14		
H I	1026	5.66 ± 3.65	3400 ± 1000	-314 ± 8
O VI	1302 Narrow	3.78 ± 0.53	656 ± 45	-494 ± 8
O VI	1302 Broad	25.7 ± 5.1	3720 ± 480	-880 ± 8
O VI	1308 Narrow	6.10 ± 0.60		
O VI	1308 Broad	13.1 ± 4.8		

Table 2. Measured and Calculated Parameters of Mrk 1044

Line	Observed Wavelength [\AA]	FWHM [km s^{-1}]	Equivalent Width [m\AA]	$\log(\text{Column})$ [cm^{-2}] ^a	$\log(\text{Column})$ [cm^{-2}] ^b	Velocity [km s^{-1}]
System 1						
Ly β	1038.5757	50 ± 12	135 ± 37	14.69	14.60	-1175 ± 8
O VI1032	1044.9335	69 ± 3	244 ± 14	$15.12^{+0.16}_{-0.14}$	$14.93^{+0.49}_{-14.93}$	-1153 ± 8
O VI1038	1050.7038	61 ± 3	210 ± 15	$15.08^{+0.14}_{-0.12}$	$14.92^{+0.08}_{-0.10}$	-1150 ± 8
N III990 ^c	1002.291			< 14.12		
N III992 ^c	1004.103			< 14.16		
Ly α ^{d,e}	1230.9819	92 ± 7	341 ± 5		$14.20^{+0.09}_{-0.12}$	-1156 ± 7
N V1239 ^d	1254.4633	71 ± 3	209 ± 8		$14.42^{+0.02}_{-0.02}$	-1143 ± 6
N V1243 ^d	1258.4999	71 ± 3	162 ± 6		$14.51^{+0.02}_{-0.03}$	-1143 ± 6
C IV1549 ^d	1567.7329	50 ± 6	204 ± 5	$13.94^{+0.02}_{-0.03}$	$14.26^{+0.23}_{-0.53}$	-1147 ± 5
C IV1551 ^d	1570.3602	47 ± 5	156 ± 4	$14.04^{+0.02}_{-0.02}$	$14.48^{+0.05}_{-0.06}$	-1143 ± 5
System 2						
O VI1032	1047.8857	24 ± 8	41 ± 10	$13.57^{+0.10}_{-0.13}$		-295 ± 8
O VI1038	1053.7330	16 ± 13	18 ± 16	$13.48^{+0.29}_{-0.89}$		-276 ± 8
N III990 ^c	1005.102			< 14.12		
N III992 ^c	1006.919			< 14.16		

^aDerived from curve of growth arguments

^bDerived from optical depth integration

^c 3σ upper limits

^dValues from F05, corrected for error in C_f

^e $C_f = 0.75$

Table 3. Galactic Absorption Features

Line	Observed Wavelength [\AA]	FWHM [km s^{-1}]	Equivalent Width [m\AA]	$\log(\text{Column})$ [cm^{-2}] ^a	$\log(\text{Column})$ [cm^{-2}] ^b	Velocity [km s^{-1}]
C II1036.337	1036.2431	83.9 ± 10.0	263 ± 33			-27 ± 8
C II*1037.018	1036.8348	236 ± 53	610 ± 180			-53 ± 8
O I1039.230	1039.2248	53.5 ± 4.2	183 ± 13	$15.75^{+0.10}_{-0.09}$	$15.56^{+0.05}_{-0.06}$	-2 ± 8
Ar I1048.220	1048.2091	17.8 ± 4.5	93 ± 14	$13.73^{+0.09}_{-0.10}$		-3 ± 8
Fe II1055.262	1055.2443	25.0 ± 4.8	58 ± 12			-5 ± 8
Fe II1063.2	1063.1610	72 ± 17	213 ± 41			-11 ± 8
H ₂				$\approx 16.9^c$		≈ 0

^aDerived from curve of growth arguments

^bDerived from optical depth integration

^cBy-eye choices fluctuated between $(7-8) \times 10^{16}$

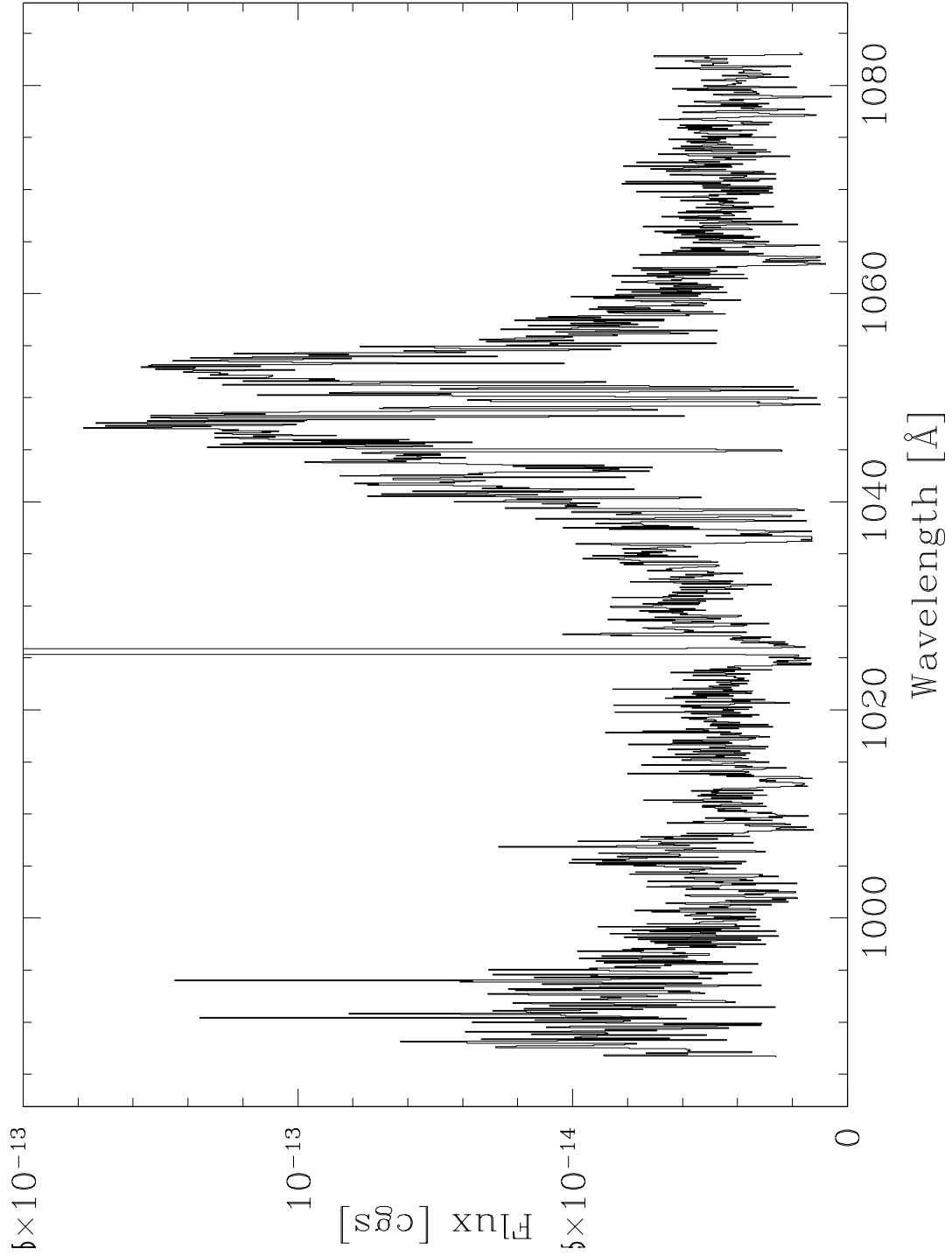


Fig. 1.— Observed FUSE spectrum of Mrk 1044. Most prominent are O VI $\lambda\lambda 1032, 1038$ and geocoronal Ly β emission lines. Less prominent are N III $\lambda\lambda 990, 992$ emission and a broad feature of excess flux at the probable redshift of Ly β .

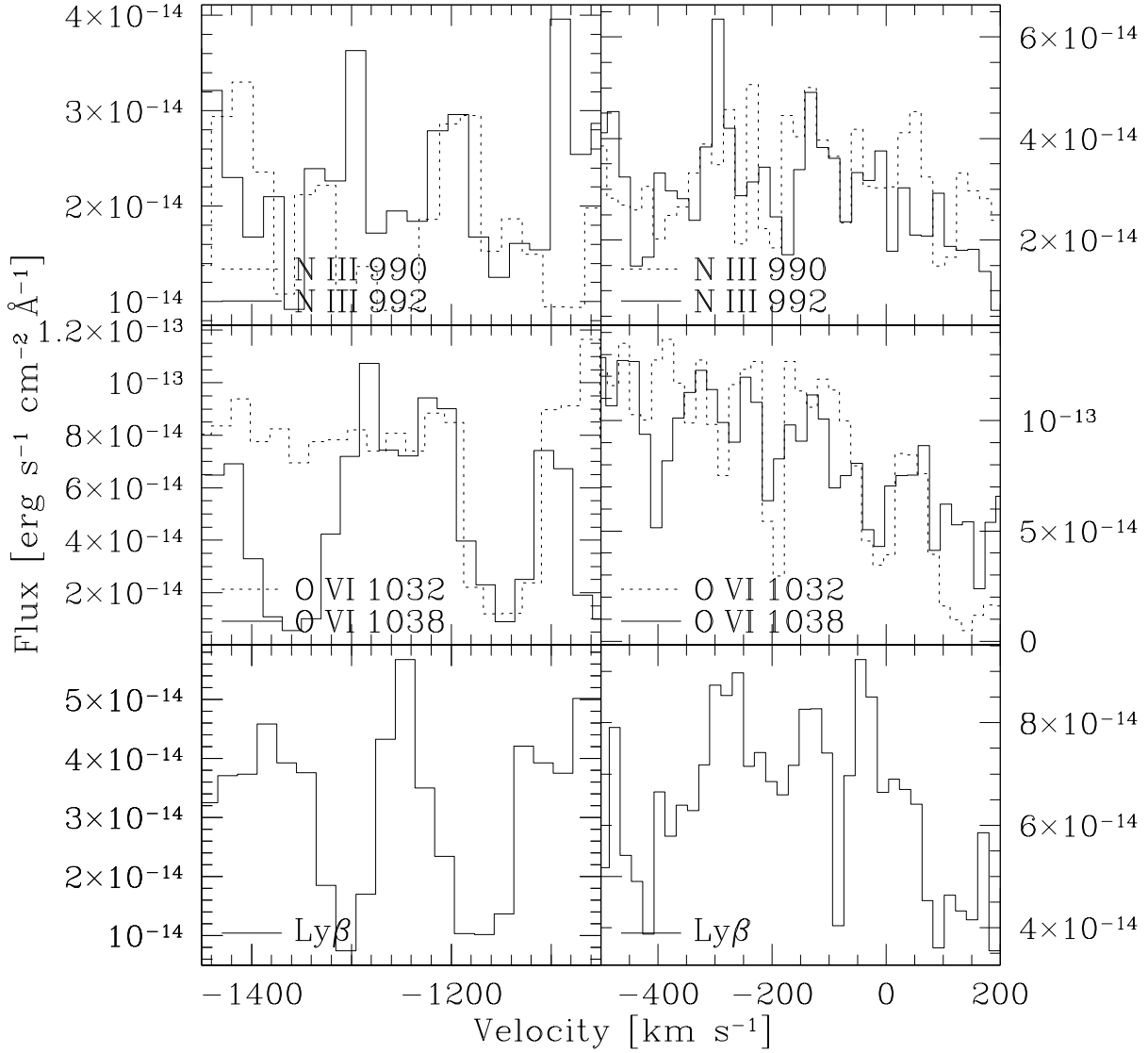


Fig. 2.— Velocity maps centered on the velocity of the absorption systems found in F05. System 1 (left) at -1158 and System 2 (right) at -286 km s⁻¹ match well with the velocities of -1158 and -286 km s⁻¹ found in F05. The line seen in Lyman β for System 1 is a blend of Lyman β and a Galactic H₂ line.

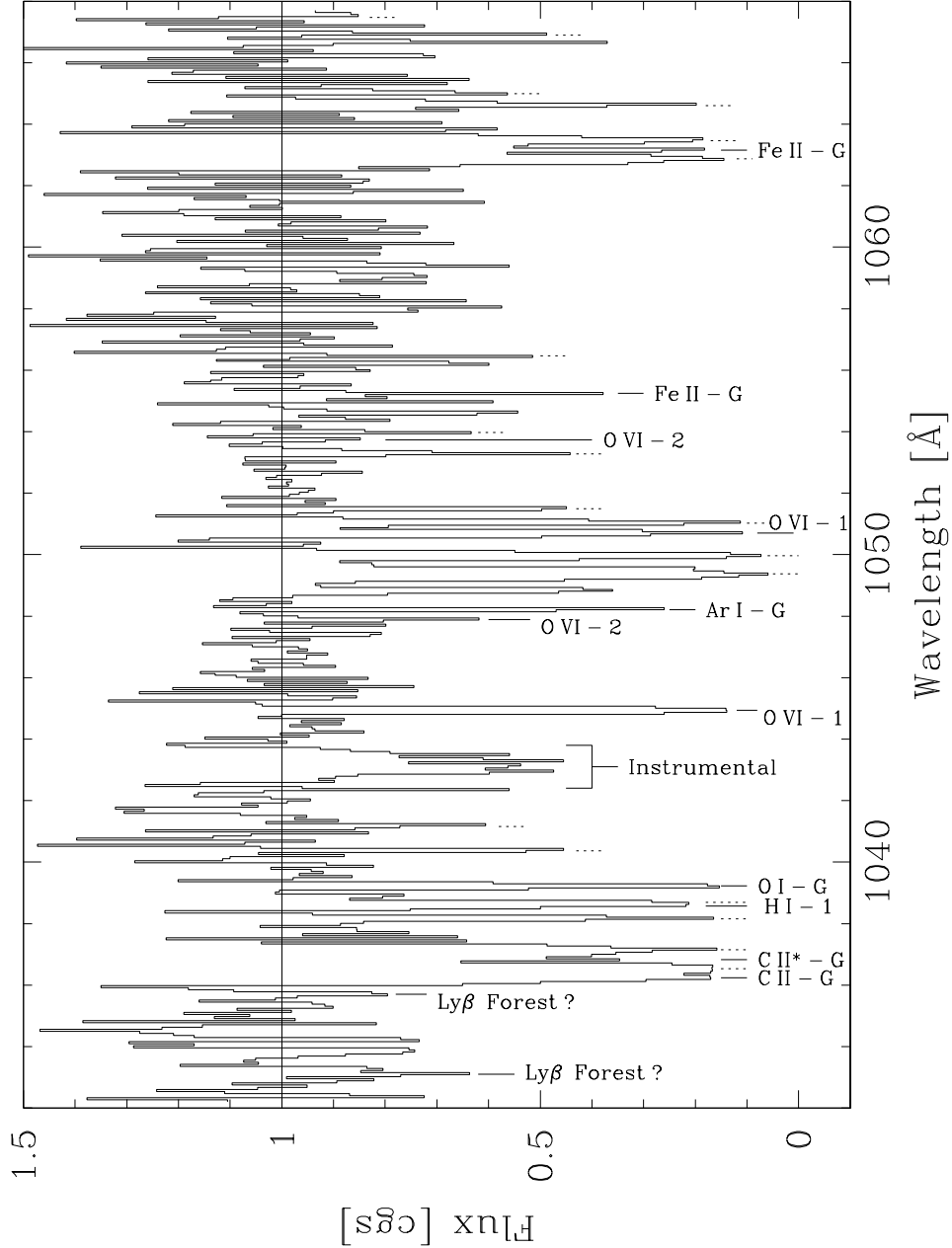


Fig. 3.— One of the flattened spectra around the O VI emission line of Mrk 1044 used for our nine pseudo-continuum fits. The H_2 subtraction has not been done with this spectrum. Identified lines and features are marked below the spectrum. Lines intrinsic to Mrk 1044 are marked by their system (1 or 2), lines belonging to Galactic sources are marked with a 'G' and H_2 lines are marked with a dotted line. The feature around 1043 Å is instrumental. The C II lines, the Ly β line for System 1, and the red Fe II line are all blended to some degree with H_2 .

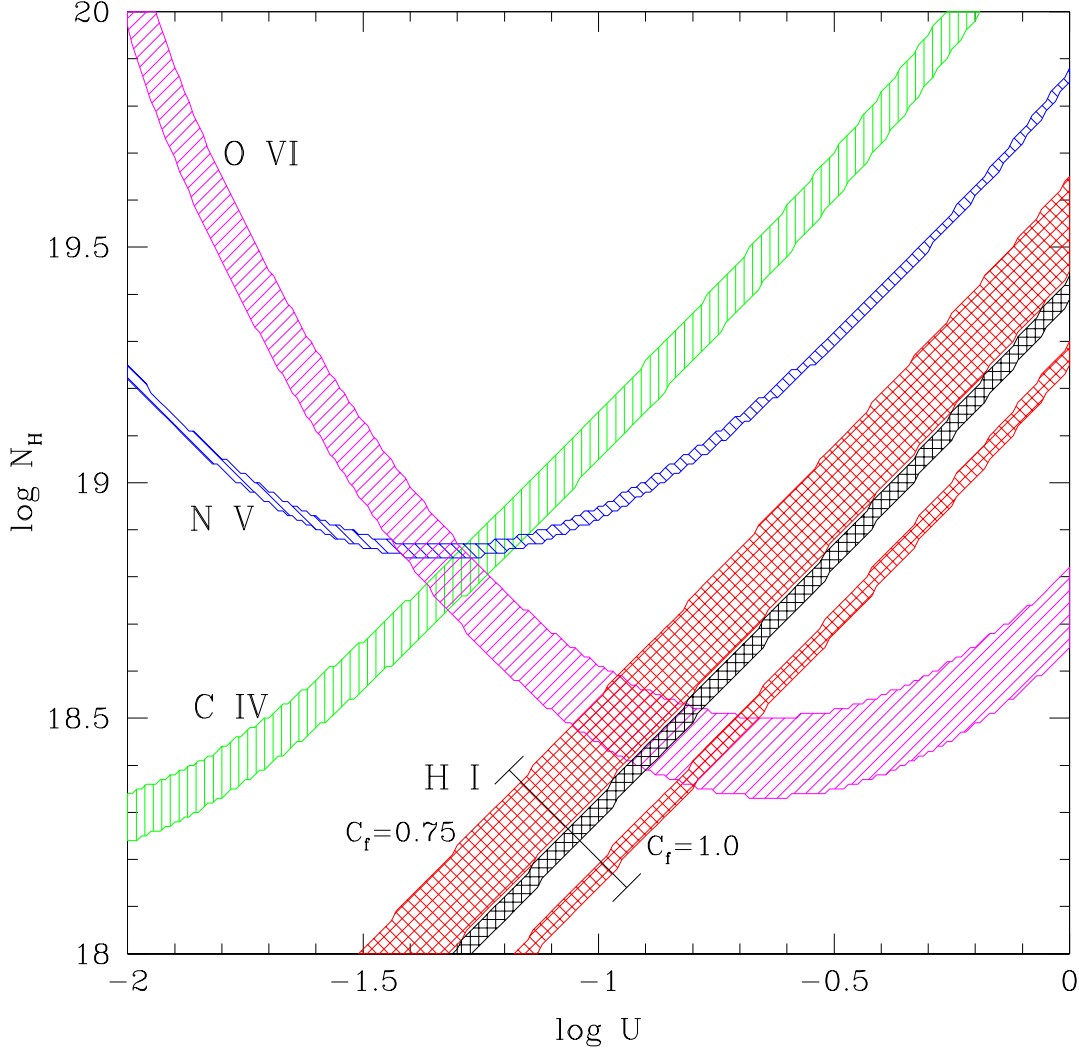


Fig. 4.— CLOUDY models with its AGN template spectrum at many $\log U$ - $\log N_H$ points assuming solar metallicity. Shaded regions indicate agreement with observed column densities of several ions at the 1σ level. Slashed shading represents agreement with the observed O VI column density, vertical shading indicates agreement with C IV, backslashed with N V, and crosshatched with H I. Because the covering fraction (C_f) parameter differs between O VI and both C IV, and N V, column densities of H I are calculated for several C_f . Shown are those for $C_f = 0.75, 0.85$ and 1.00 , with the lower covering fraction preferring a higher N_H . The range of models in agreement (the thickness of the band) with H I is relatively constant down to about $C_f = 0.80$. Below this, the uncertainty in the column density rises dramatically because the depth of the Ly α line is ≈ 0.75 in terms of normalized flux. See Fig. 4 of F05 for an example of the normalized spectrum around Ly α . The metal lines all agree in a small region of parameter space around $\log U = -1.29, \log N_H = 18.85$. The vertical distance between this point and the preferred model for H I is about $+0.7$, between the metal-selected model and just the 1σ envelope of H I is about $+0.6$.

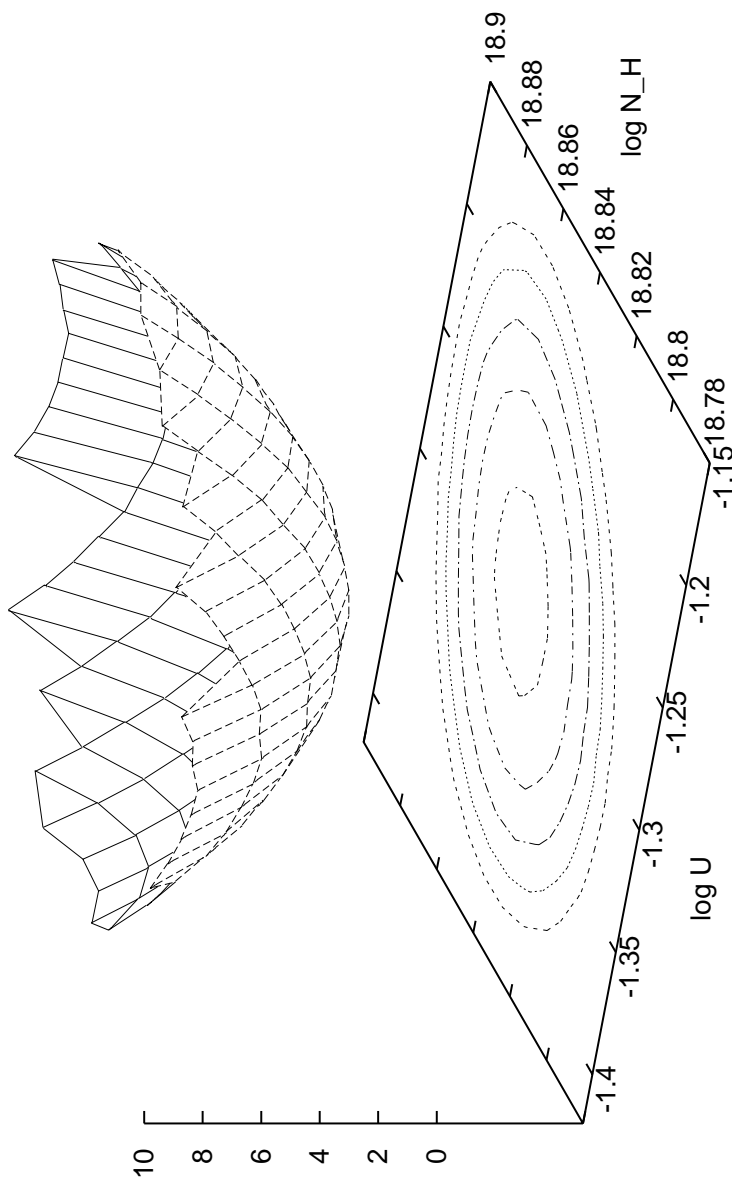


Fig. 5.— The χ^2 surface for Cloudy models at solar metallicity compared to observed column densities of H I, C IV, N V, and O VI. The surface is shown up to a χ^2 of 10, and the curves of constant χ^2 (2, 4, 6, 8, and 10) are projected into the $\log U$ - $\log N_H$ plane. The H I component of the fit has been shifted by -0.71 dex to match the metal’s minimum at $\log U = -1.29$, $\log N_H = 18.85$. This implies a metallicity of $+0.71$ and thus a corrected $\log N_H$ of 18.14.

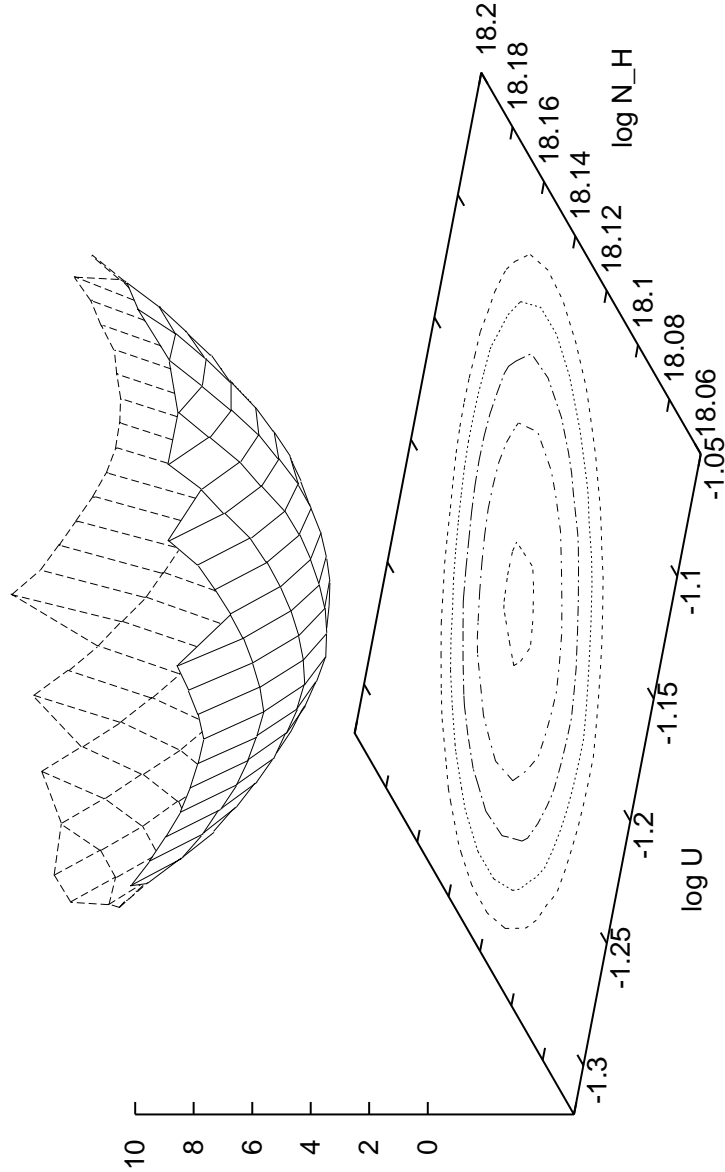


Fig. 6.— The χ^2 surface for Cloudy models at a bulk metallicity of five times solar with a solar mixture in metals and Helium enhanced by $\Delta Y/\Delta Z = 2$ compared to observed column densities of H I, C IV, N V, and O VI. The surface is shown up to a χ^2 of 10, and the curves of constant χ^2 (2, 4, 6, 8, and 10) are projected into the $\log U$ - $\log N_H$ plane. The minimum lies at $\log U = -1.20$, $\log N_H = 18.13$, only slightly different than the inferred values from Figure 5.